

Article

Grinding Kinetics Study of Tungsten Ore

Jennire V. Nava¹, Alfredo L. Coello-Velázquez² and Juan M. Menéndez-Aguado^{1,*} 

¹ Escuela Politécnica de Mieres, Universidad de Oviedo, C/Gonzalo Gutiérrez Quirós, 33600 Mieres, Asturias, Spain; jvanessanavar@gmail.com

² CETAM, Universidad de Moa Dr. Antonio Núñez Jiménez, Moa 83300, Cuba; acoello@ismm.edu.cu

* Correspondence: maguado@uniovi.es

Abstract: The European Commission (EC) maintains the consideration of tungsten as a critical raw material for the European industry, being the comminution stage of tungsten-bearing minerals an essential step in the tungsten concentration process. Comminution operations involve approximately 3–4% of worldwide energy consumption; therefore, grinding optimization should be a priority. In this study, the grinding behavior of tungsten ore from Barruecopardo Mine (Salamanca, Spain) is analyzed. A protocol based on Austin's methodology and PBM is developed in order to study the influence of operational and geometallurgical variables on grinding kinetics. In addition to the kinetic parameters, the breakage probability (S_i) and breakage function (B_{ij}) is determined. The selection function was formulated for the Barruecopardo Mine with respect to the mill speed.

Keywords: critical raw materials; tungsten ore; grinding kinetics



Citation: Nava, J.V.; Coello-Velázquez, A.L.; Menéndez-Aguado, J.M. Grinding Kinetics Study of Tungsten Ore. *Metals* **2021**, *11*, 71. <https://doi.org/10.3390/met11010071>

Received: 28 November 2020

Accepted: 29 December 2020

Published: 31 December 2020

Publisher's Note: MDPI stays neutral with regard to jurisdictional claims in published maps and institutional affiliations.



Copyright: © 2020 by the authors. Licensee MDPI, Basel, Switzerland. This article is an open access article distributed under the terms and conditions of the Creative Commons Attribution (CC BY) license (<https://creativecommons.org/licenses/by/4.0/>).

1. Introduction

The European Union has recently published the updated list of critical raw materials, in which tungsten (W) is included. This critical condition is defined by both the supply risk to the EU and the economic importance developed on the industrial value chains of the European Union [1].

Tungsten presents strategic applications on high strength alloys for machining tools, automotive and mobile phone sectors, among others [2]. Currently, there are several tungsten mines in Europe, some active and others on the exploration stage [3]. This is the case of the Barruecopardo mine in Salamanca (Spain), owned by Ormonde Mining PLC and currently administered by Saloro S.L., which is estimated to provide 11% of the non-Chinese global supply of tungsten [4]. The main minerals present in Barruecopardo are scheelite (CaWO_4) and wolframite ($(\text{Fe}, \text{Mn})\text{WO}_4$), which constitute the ore. Arsenopyrite (FeAsS), pyrite (FeS_2), chalcopyrite (CuFeS_2), and ilmenite (FeTiO_3) are also present as primary minerals of the gangue [5,6].

Regarding mineral benefit, the comminution stage represents 3–4% of the energy consumption worldwide and 40–70% of the energy consumed in a mineral processing plant [7,8]. In fact, ball-mill grinding is one of the most energy-consuming techniques. Therefore, setting the optimal values of the operational and mineralogical parameters both for the initial design and the process adaptation to ore variations [9].

Several researchers have investigated the influence exerted on kinetic conditions by operational parameters such as mill speed [10,11] and filling volume [12,13]. Other researchers devoted their work to study geometallurgical variables such as grain size, shape and roughness, specific surface area, orientation, hardness, fracture strength, feed particle size distribution, and mineralogy [14–20] using optical microscopy or more advanced techniques, such as Quantitative Microstructural Analysis (QMA) [21]. Consequently, a small improvement in machinery efficiency and an optimal design in the grinding system, taking into account the optimization of the above-mentioned parameters, would greatly cut down plant operational costs, impacting environmental issues and resource management [22,23].

This work aims to characterize the grinding kinetic behavior at a lab-scale of tungsten ore, due to its importance as a critical raw material to the EU, by determining the kinetic parameters following the Austin model. A second objective is to assess the influence of mill speed on the kinetic and geometallurgical parameters, being mill speed the more easily adjustable operational parameter at an industrial scale.

2. Theoretical Background

The population balance model (PBM) has been widely used in ball mills since its proposal by Austin [24]. This model is based on determining the particle size distribution grouped in size classes. A mass balance for the class i in a well-mixed grinding process is done by employing Equation (1), where a first-order kinetic fragmentation is assumed.

$$\frac{dw_i}{dt} = -S_i w_i(t) + \sum_{j=1}^{i-1} b_{ij} k_j w_j(t) \quad (1)$$

where $w_i(t)$ is the remnant mass fraction of particle size class i at grinding time t . The first term of the right-hand side is the mass fraction of the monosize i particles that break and thus no longer belong to that monosize, being S_i the probability of fracture. The second term represents the contribution of all monosizes coarser than i that break to produce particles of monosize i . The fracture rate of a monosize material can be expressed by Equation (2):

$$\frac{-dw_i}{dt} = S_i w_i(t) \quad (2)$$

where S_i is the probability of fracture or specific fracture rate, whose unit is t^{-1} . Assuming that S_i does not change with time, the integral results in Equation (3).

$$\text{Log}(w_i(t)) - \text{Log}(w_i(0)) = \frac{-S_i(t)}{2.3} \quad (3)$$

where w_i is the weight fraction of mineral feed into the mill having a size 1 for time t , and S_i is the probability of fracture. According to the methodology proposed by Austin et al. [25], once S_i values have been obtained through slope determination, they are plotted to the particle size, and Equation (4) is proposed to study the behavior of the probability of fracture S_i .

$$S_i = \alpha_T X_i^\alpha \quad (4)$$

where X_i is the upper size limit of the interval in mm, and α_T and α are model parameters that depend on the material properties and the grinding conditions. To find the second term of Equation (1), the fracture function b_{ij} is defined. This function represents the particle fraction that belongs initially to interval j , after fracture falls in interval i . It is recommended to represent this value in cumulative form B_{ij} , whose calculation is done with Equation (5).

$$B_{ij} = \sum_{k=n}^i b_{kj} \quad (5)$$

That is, B_{ij} is the sum of the mineral fractions finer than the upper limit of interval i as a result of the primary break of the size interval j . Austin et al. [25] showed that B_{ij} values could be estimated from a size analysis of the products over short grinding times of an initial feed chiefly of size j through the method *BII* [25–27]. With the parameters of fracture function, B_{ij} can be determined graphically through an empirical function like Equation (6).

$$B_{ij} = \phi_j \left(\frac{X_{i-1}}{X_j} \right)^\gamma + (1 - \phi_j) \left(\frac{X_{i-1}}{X_j} \right)^\beta \quad n \geq i \geq j + 1 \quad (6)$$

where ϕ_j , γ and β are parameters that depend on the material properties. The critical speed, N_c , is calculated using Equation (7).

$$N_c = \frac{42.3}{\sqrt{D-d}} \quad (7)$$

where D is the mill diameter and d is the ball diameter [m]. Ball mill filling volume is calculated using Equation (8).

$$J = \left(\frac{\text{mass of balls}}{\text{ball density} \times \text{mill volume}} \right) \times \frac{1.0}{0.6} \quad (8)$$

On the other side, Austin and Brame [28] calculated the sorting function α_T in a general way through Equation (9).

$$\alpha_T = \frac{v_c - 0.1}{1 + e^{[15.7(v_c - 0.94)]}} \quad (9)$$

where v_c is the mill speed expressed as a fraction of the critical speed. Finally, according to [29], the Froude number expresses the ratio of centrifugal acceleration to gravity acceleration at the perimeter of the mill chamber (Equation (10)). This number can be used to characterize the charge motion in the mill and the ball regime. Thus, in laboratory ball mills, it is recommended to define work conditions with centrifugal acceleration at the shell equalling $1/2$ of the acceleration due to gravity ($F_r = 0.5$), corresponding to $v_c = 70.7\%$ [29].

$$F_r = \frac{\frac{D}{2}\omega^2}{g} = \frac{2\pi^2 n^2 D}{g} \quad (10)$$

3. Materials and Methods

3.1. Sample Preparation and Feed Characterization

The sample mineralogy was extensively characterized by Alfonso et al. [6]. A representative sample from an old waste dump of the Barruecopardo mine was prepared in a 4 mm jaw crusher. After homogenization and quartering using a riffle splitter, sieving provided an adequate quantity of the following size intervals, which will be considered as monosizes in this work: 5000/4000, 4000/3350, 3000/2000, 2000/1000, 1000/500, 500/250, 250/125, 125/75, 75/45 μm .

A representative sample was characterized chemically through XRF, using a Bruker XRF S-4 Pioneer Advance, with sample preparation in a Claisse Perler, model M-4.

3.2. Calculation of Critical Speed and Initial Conditions for the Grinding Kinetic Tests

Mill critical speed was calculated using Equation (7). Table 1 shows the three milling speeds used in the tests.

Table 1. Mill rotation speeds used in the grinding kinetic tests.

Mill Speed	n [rpm]	Froude Number
N_c ($v_c = 1$)	112.3	1
N_1 ($v_c = 0.6$)	67.4	0.43
N_2 ($v_c = 0.7$)	78.6	0.58
N_3 ($v_c = 0.8$)	89.9	0.76

Grinding kinetic tests were run in a laboratory mill, 17.8 cm in diameter and 4500 cm³ in capacity. Feed was of 900 cm³, and milling load consisted of 6.6 kg of steel balls with the following ball size distribution: 45 balls 19 mm in diameter, 23 balls 29.7 mm in diameter, and 17 balls 36.8 mm in diameter. Fill fraction was calculated using Equation (8). The feed consisted of samples of the 9 monosizes selected (5000/4000, 4000/3000, 3000/2000, 2000/1000, 1000/500, 500/250, 250/125, 125/75, 75/45 μm). Grinding times were 0.5, 1,

1.5, 3.5, 6.5, and 10.5 min. Each sample was dumped and, after performing a grain size analysis, W content was measured to assess the evolution of the W grade with respect to the kinetic parameters.

3.3. Determination of Fracture Probability (S_i), Fracture Function (B_{ij}), and the Kinetic Parameters (α_T , α , ϕ_j , γ , and β)

3.3.1. Fracture Probability (S_i) and Kinetic Parameters (α_T , and α)

After obtaining the oversize weights for each grinding time, and plotting the time function $\log(w_i(t)/w_i(0))$ for each monosize, the equation for each curve, and consequently, the S_i value, were calculated through the linear fitting using Equation (3). Then, S_i values for each monosize were plotted, and the parameters (α_T and α) were calculated using Equation (4) for each mill speed condition to study the influence of this operational variable on the probability of fracture and on the kinetic parameters α_T and α . The selection function α_T , obtained through Equation (9) was calculated using an equation designed for this particular ore, as detailed in Section 4.2.

3.3.2. Determination of the Fracture Function (B_{ij}) and the Kinetic Parameters (ϕ_j , γ and β)

These calculations were done for each feed monosize, i , at each mill speed condition and after the grinding time. Product particle size analysis was done by sieving with mesh sizes i to $j-n$. Weight of oversizes i and S_{j-n} was determined, and fracture function values b_{ij} and cumulative value B_{ij} , were obtained using Equation (5). Finally, B_{ij} data were plotted to relative size j/i for each monosize and mill speed conditions. The rest of the kinetic parameters were calculated through Equation (6).

3.4. Study of P_{80} and the Ratio of Reduction R_r

The evolution of some relevant parameters of the product was represented. These parameters were P_{80} and the ratio of reduction, R_r , after a 0.5 min grinding time at several mill speeds for each feed monosize. Likewise, the evolution of the probability of fracture, S_i , and R_r with mill speed was studied, for each feed monosize.

3.5. Chemical Characterisation of the Product

Milling products were chemically characterized with the equipment specified in Section 3.1.

4. Results and Discussion

4.1. Feed Characterization

The sample mechanically prepared displays a particle size distribution (PSD), as shown in Figure 1.

F_{80} for the Barruecopardo sample is 1690 μm . Table 2 shows W contents obtained from a mineralogical study for each size interval.

Table 2. Fractional results of XRF (ND = not detected).

Size Interval (μm)	Weight (%)	W (ppm)	STD (ppm)
>4000	1.79	ND	-
3350–4000	3.93	ND	-
2000–3350	9.71	ND	-
1000–2000	29.53	40	10
500–1000	24.01	105	13
250–500	19.94	146	13
125–250	8.23	75	12
75–125	1.52	23	10
45–75	0.78	ND	-
<45	0.55	ND	-

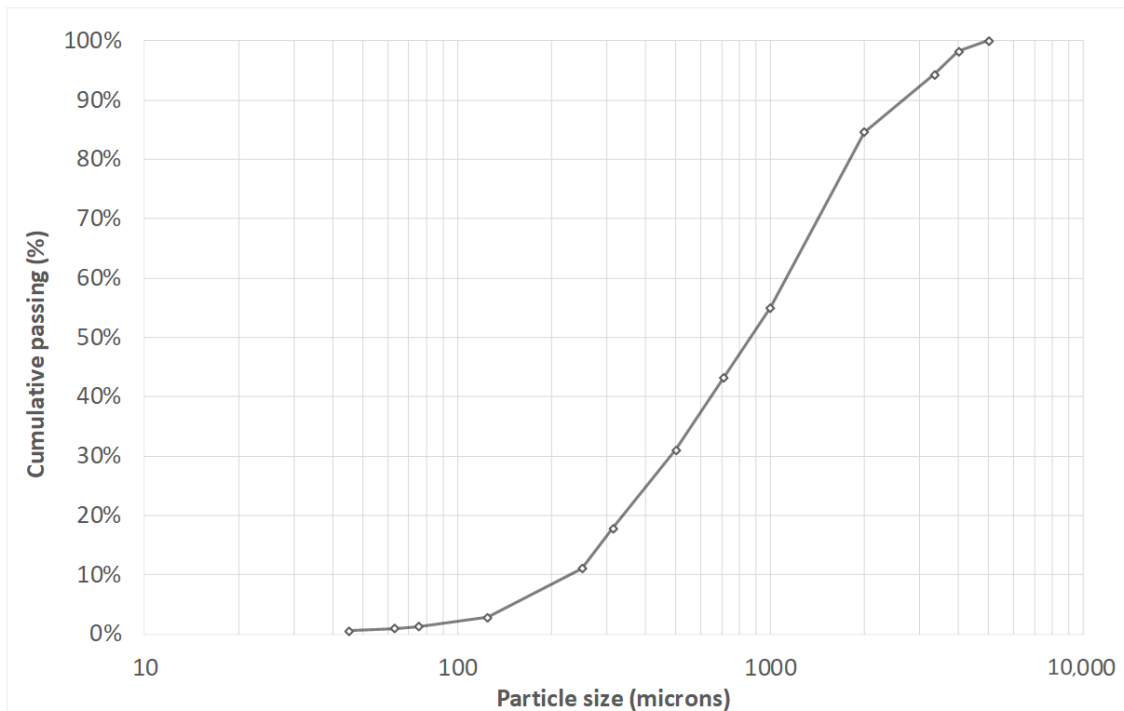


Figure 1. PSD for the Barruecopardo ore head samples.

W contents shown in Table 2 reflect that the sample comes from a waste dump of the Barruecopardo mine, and therefore from an area with low W contents.

The probability of fracture (S_i) and the kinetic parameters (α , α_T), a size of 80% of product undersize (P_{80}), and the reduction ratio were obtained from this procedure (R_r):

Figure 2 shows the values (S_i) plotted to the particle size according to the mill speed.

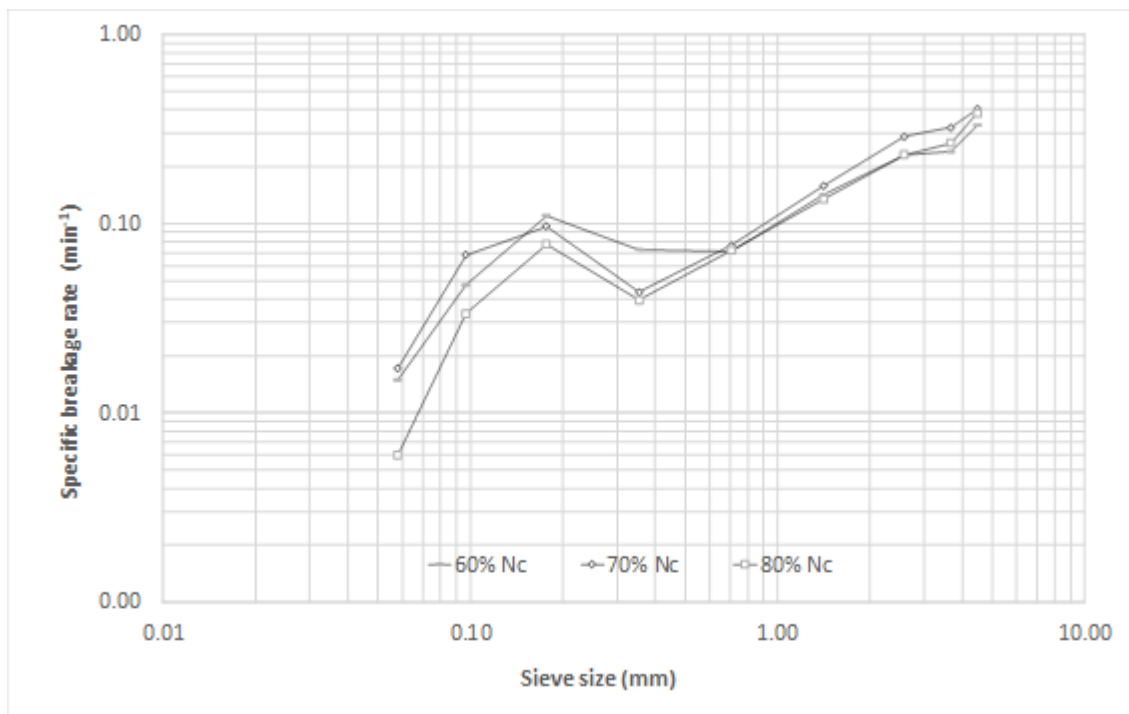


Figure 2. Evolution of the probability of fracture (S_i) with particle size, in relation to mill speed.

Figure 2 shows that comparing the three speeds tested, the highest probability of fracture occurred at 70% critical speed, agreeing with Gupta and Sharma [9], Gupta [10], and Herbst and Fuerstenau [30], who did their experiments at lab scale, with several materials, simulations, and finally upscaling. This also verified the Steiner [29] recommendation of a configuration with F_r value close to 0.5. For intermediate and coarse grain sizes, a rather linear trend was observed using a logarithmic scale. This coincided with Deniz [22] for this grain size interval.

Noteworthy was a sharp break in slope that occurred at around 250 μm for the three tested speeds, coinciding with the size fractions more enriched in W, as shown in Table 2. Moreover, the results backed Gupta and Sharma's [9] statements, pointing to the probability of fracture S_i being one of the mill operational conditions more influenced by the mineralogical variability among monosize fractions.

On the other side, the evolution of S_i , P_{80} , and R_r for each feed monosize was studied at different mill speeds as summarized in Table 3. The reduction ratio was the result of dividing the d_{80} in the feed size (F_{80}) by the d_{80} in the product size (P_{80}).

Table 3. S_i , R_r , and P_{80} values as a function of working speed for each monosize.

Monosize (μm)	Specific Rate of Breakage, S_i (1/min)			Reduction Ratio, R_r			P_{80} (μm)		
	60% N_c	70% N_c	80% N_c	60% N_c	70% N_c	80% N_c	60% N_c	70% N_c	80% N_c
5000/4000	0.331	0.403	0.383	2.14	2.59	2.38	2244.9	1856.6	2014.7
4000/3350	0.241	0.322	0.266	1.66	2.08	1.74	2329.4	1864.2	2220.5
3350/2000	0.231	0.289	0.232	1.92	2.13	1.85	1608.1	1447.7	1665.0
2000/1000	0.143	0.159	0.135	1.67	1.84	1.69	1078.5	977.2	1063.8
1000/500	0.071	0.077	0.072	1.13	1.14	1.13	792.9	786.1	799.7
500/250	0.073	0.043	0.039	1.11	1.06	1.05	406.0	425.8	427.9
250/125	0.110	0.097	0.078	1.18	1.17	1.10	191.1	192.3	204.6
125/75	0.047	0.068	0.033	1.04	1.07	1.03	110.2	107.8	111.9
75/45	0.015	0.017	0.006	1.01	1.01	1.01	68.4	68.1	68.2

It must be highlighted in Table 3 that once the total grinding time was reached, a finer P_{80} and a higher R_r were obtained at 70% working speed for most of the monosizes. This confirmed that the mill speed affected the grinding product [11,31].

The kinetic parameters (α , α_T) obtained after linearization of Equation (4) are summarized in Table 4 and the selection function is represented in Figure 3.

Table 4. Values of the kinetic parameters α , α_T for different mill speeds.

	60% N_c	70% N_c	80% N_c
α	0.42	0.58	0.74
α_T (1/min)	0.14	0.14	0.11

Table 4 shows that the parameter α is coherent with what Austin et al. [25] reported. These authors pointed out that it usually ranges between 0.5 and 1.5 and that it depends only on the mineral. On the other side, Table 4 and Figure 3 show that the value of the selection function α_T does not vary significantly despite the increasing speed, because the mill geometry remains unchanged. Figure 4 displays α_T values calculated from Equation (9), as proposed by Austin and Brame [28]. It can be seen that this expression does not fit this case. This led to a polynomial adjustment using the experiment values, as it was shown in Equation (11) that it fitted better with the studied sample.

$$\alpha_T = -1.775 v_c^2 + 2.3625 v_c - 0.6402 \quad (11)$$

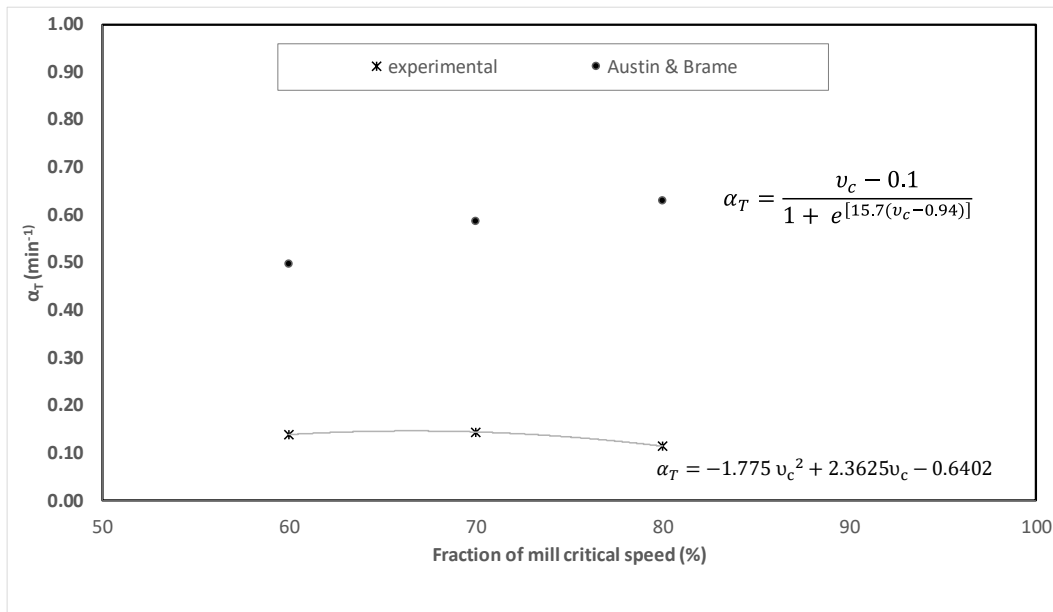


Figure 3. Variation of α_T with the working speed fraction.

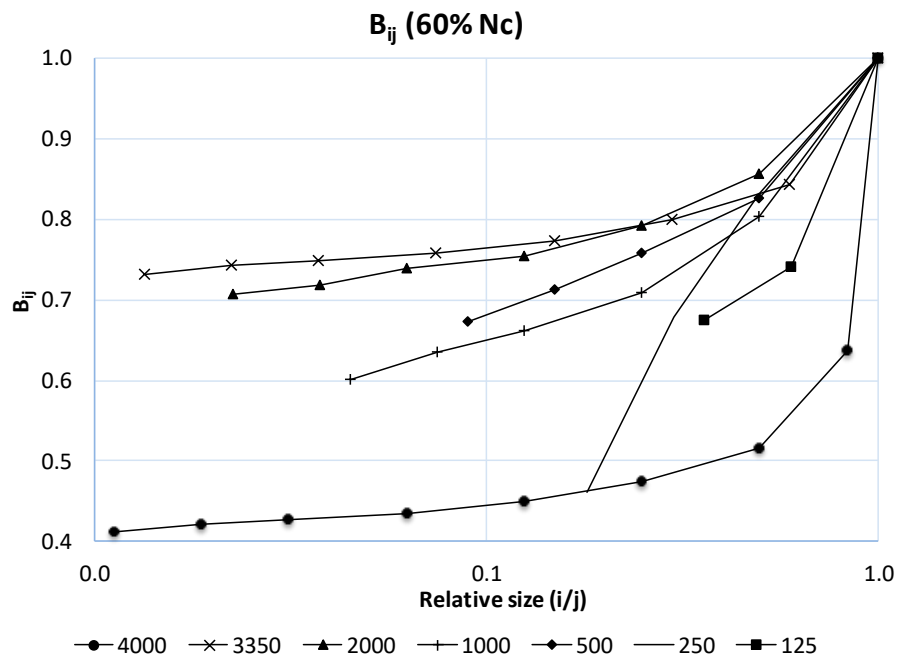


Figure 4. Behavior of the fracture function (B_{ij}), with respect to particle size. 60% working speed N_c (Barruecopardo ore).

4.2. Fracture Function, Kinetic Parameters (ϕ_j , γ and β)

The values of fracture function B_{ij} in relation to the particle size for each monosize as the mill speed varied were determined through Equation (5) and are shown in Figures 4–6 for 60%, 70%, and 80% mill speed, respectively.

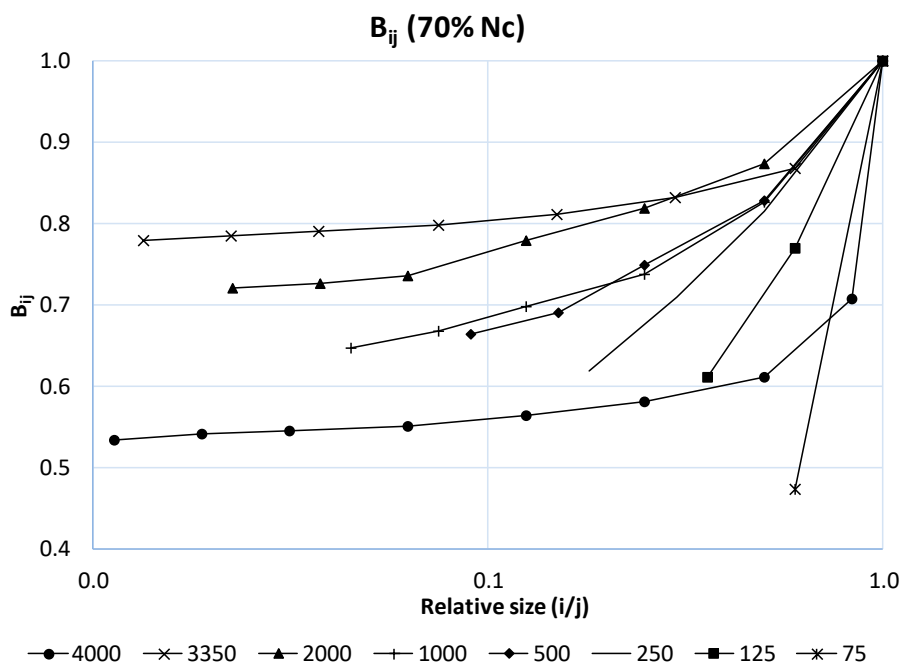


Figure 5. Behavior of the fracture function (B_{ij}), with respect to particle size. 70% working speed N_c (Barruecopardo ore).

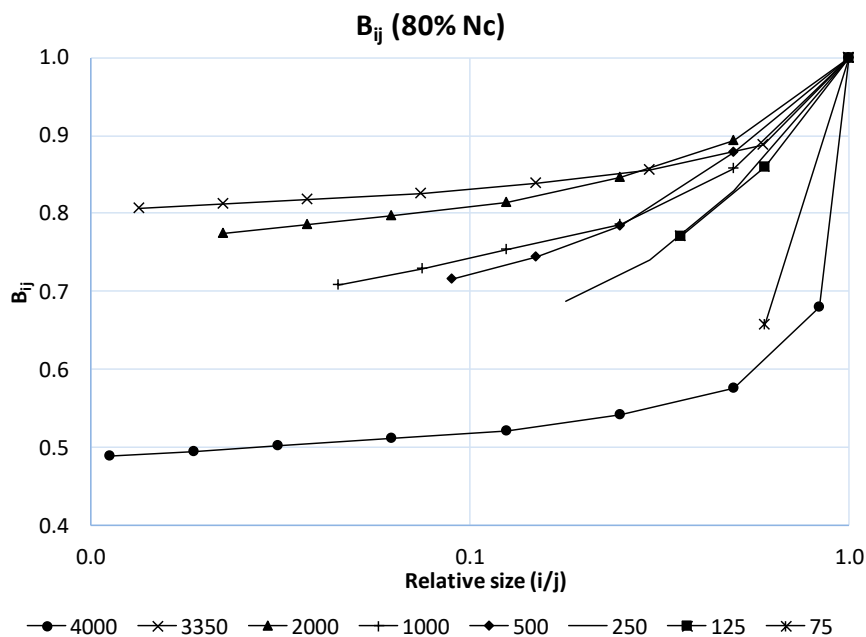


Figure 6. Behavior of the fracture function (B_{ij}), with respect to particle size. 80% working speed N_c (Barruecopardo ore).

The kinetic parameters of fracture function (ϕ_j , γ , and β) are shown in Table 5. According to Austin et al. (1984), ϕ_j and β are parameters that depend on the material. Regarding γ and β , these authors propose that their values were usually in the range of 0.5–1.5 and 2.5–5.0, respectively.

Table 5. Values of the kinetic parameters (φ_j , γ , β) for each monosize and for different mill speed conditions.

Monosize (μm)	j	j/i	60% N_c			70% N_c			80% N_c					
			B_{ij} (Test)	φ_j	γ	β	B_{ij} (Test)	φ_j	γ	β	B_{ij} (Test)	φ_j	γ	β
4000	4000	1.000	1.000				1.000				1.000			
	3350	0.838	0.637				0.708				0.680			
	2000	0.500	0.516				0.612				0.576			
	1000	0.250	0.474				0.581				0.542			
	500	0.125	0.450	0.483	0.036	3.285	0.563	0.586	0.021	3.361	0.522	0.552	0.027	3.477
	250	0.063	0.435				0.551				0.512			
	125	0.031	0.426				0.545				0.503			
	75	0.019	0.421				0.540				0.495			
45	0.011	0.411				0.534				0.489				
3350	3350	1.000	1.000				1.000				1.000			
	2000	0.597	0.844				0.869				0.888			
	1000	0.299	0.799				0.833				0.856			
	500	0.149	0.774				0.812				0.838			
	250	0.075	0.758	0.805	0.022	2.732	0.799	0.828	0.015	2.507	0.825	0.861	0.015	2.734
	125	0.037	0.749				0.791				0.818			
	75	0.022	0.743				0.785				0.812			
	45	0.013	0.731				0.779				0.807			
2000	2000	1	1				1				1			
	1000	0.5	0.856				0.875				0.893			
	500	0.25	0.793				0.818				0.845			
	250	0.125	0.755	0.840	0.047	1.905	0.779	0.874	0.055	3.123	0.814	0.882	0.035	1.862
	125	0.062	0.738				0.736				0.798			
	75	0.037	0.719				0.726				0.786			
	45	0.022	0.707				0.721				0.774			
1000	1000	1	1				1.000				1.000			
	500	0.5	0.803				0.826				0.857			
	250	0.25	0.708				0.738				0.785			
	125	0.125	0.662	0.807	0.094	2.048	0.698	0.821	0.078	1.885	0.753	0.855	0.061	1.939
	75	0.075	0.635				0.668				0.729			
	45	0.045	0.601				0.647				0.707			
500	500	1	1				1.000				1.000			
	250	0.5	0.826				0.829				0.879			
	125	0.25	0.757	0.887	0.115	4.054	0.750	0.876	0.118	2.538	0.783	0.882	0.087	1.283
	75	0.15	0.712				0.691				0.743			
	45	0.09	0.673				0.665				0.716			

Figures 4–6 and Table 5 show that B_{ij} depends on the feed grain size for parameters of 60%, 70%, and 80% of critical speed. The influence that mill speed exerts on B_{ij} , can also be noticed by comparing the different monosizes: a greater difference existed for coarser sizes, whereas it was lesser for finer sizes. This was due to the fact that coarse sizes not only possessed a higher S_i , but also were more prone to yield new finer particles (progeny). That meant that B_{ij} depended on the feed particle size, as Ipek and Goktepe [32] observed, which was also influenced by the mill speed, and concurred with results by Deniz [22]. Nevertheless, this variation was not as significant as reported by Austin et al. [25].

Table 5 shows parameter γ , which represents the fineness factor. In Figure 7, the γ values are plotted against mill speed for two feed particle sizes (4000 and 500 μm , respectively).

Figure 7 depicts that γ values are influenced by both mill speed and feed particle size. Smaller γ values were related to coarse particles (4000 μm), which meant that more fine particles were generated. Conversely, finer particles (500 μm) generated a lesser proportion of fine particles, agreeing well with results by Ipek and Goktepe [32] and Austin et al. [25].

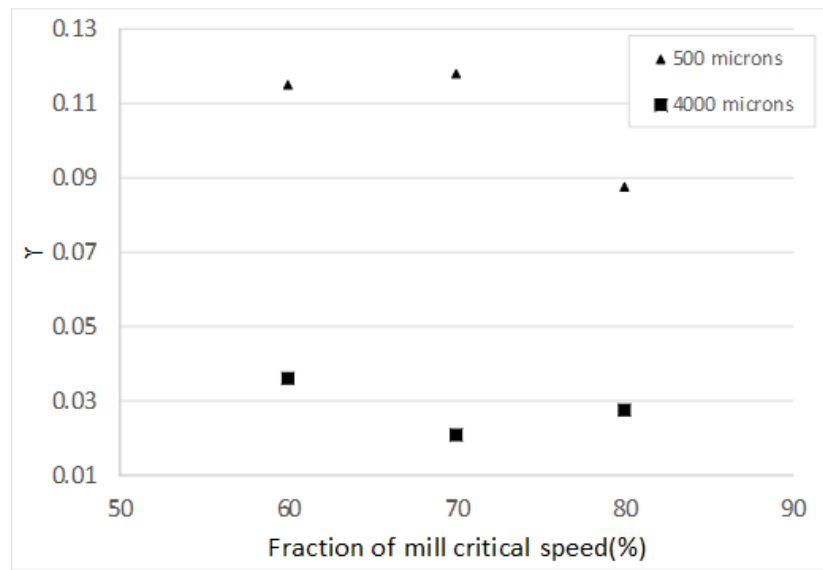


Figure 7. Variation of γ with mill speed.

4.3. Chemical Characterization of the Grinding Products

Figures 8–10 illustrate the evolution of W content in the product in relation to the feed monosizes and their grain size fractions for each mill speed.

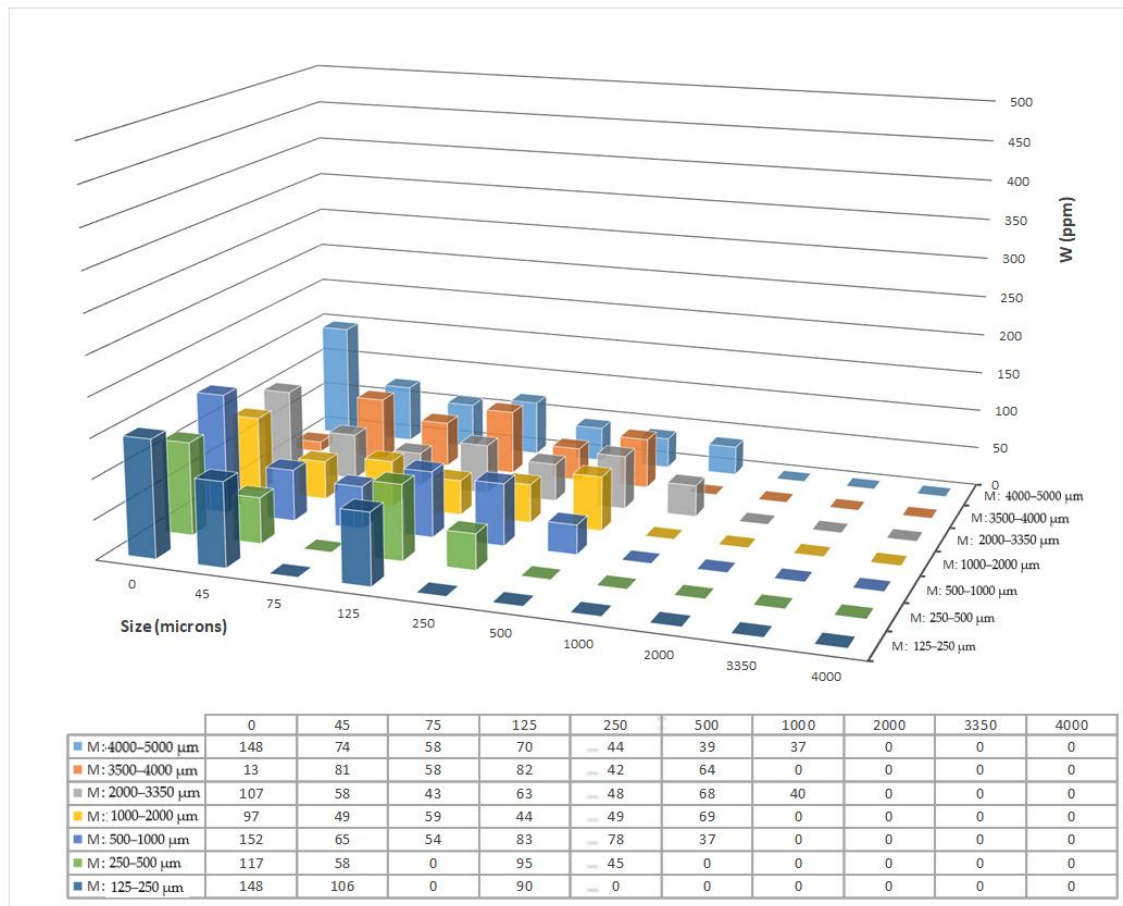


Figure 8. Evolution of the W grade in the product with respect to the monosizes and their grain size fractions for 60% Nc.

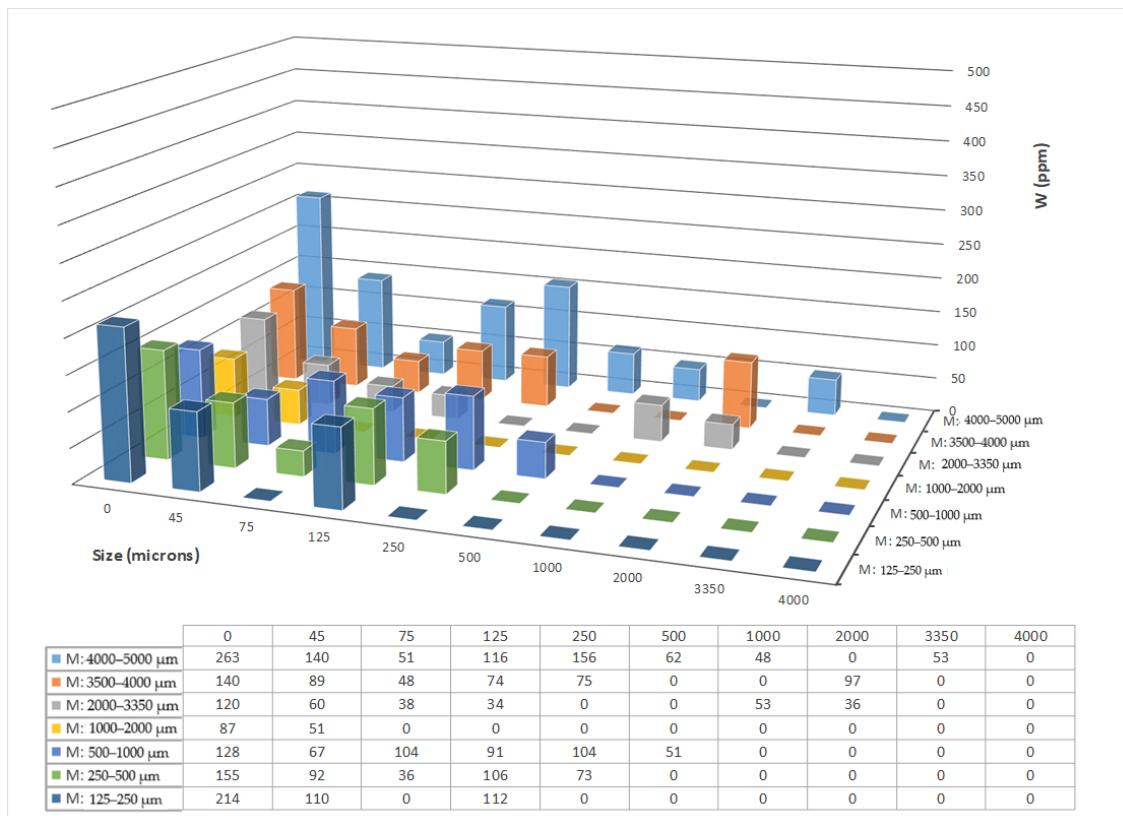


Figure 9. Evolution of the W grade in the product with respect to the monosizes and their grain size fractions for 70% Nc.

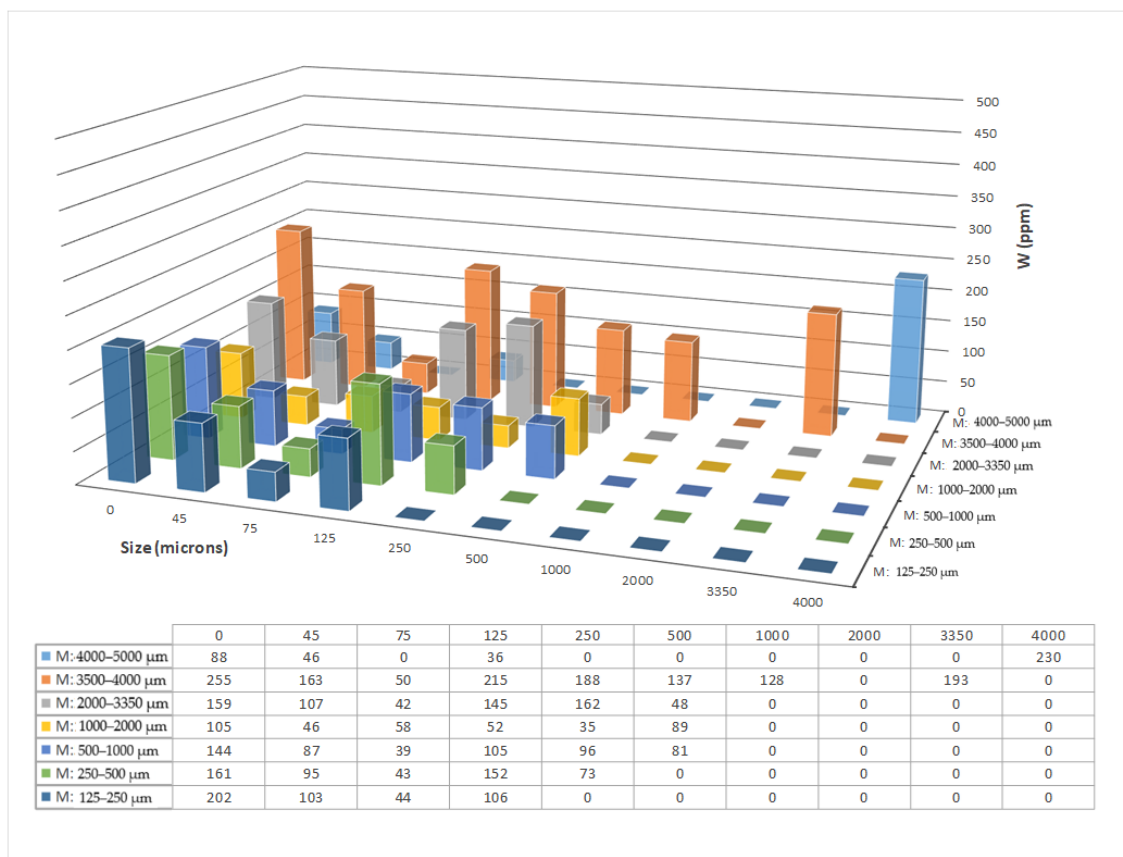


Figure 10. Evolution of the W grade in the product with respect to the monosizes and their grain size fractions for 80% Nc.

As can be seen in Figures 8–10, for most monosizes, W content increased with decreasing particle size. This could be partly explained because feed grain sizes around 250 μm already yielded higher W content, as shown in Table 2. Nevertheless, maximum values after grinding were 6–7 times higher than original values pointing undoubtedly to a differential grinding effect leading to W mineral grains mainly falling in the 250–125 μm interval. The accumulation of these W -enriched particles, which were more difficult to grind, supports the mineralogical explanation of the aforementioned breakage probability reduction at 250 μm size. In addition, this interval always presented S_i values higher than the coarser and finer intervals. This would suggest that particles of this size would have a higher probability of fracture compared to the adjacent size intervals. Indeed, in all cases, a decrease in W content could be observed down to 75 μm size, followed by an increase of further finer particles. It must be highlighted that the highest W content was yielded for grinding at 70% N_c . This could be explained because, under these grinding conditions, the mill performance was more efficient due to a more adequate charge regime (F_r close to 0.5), leading to better grinding kinetics.

5. Conclusions

The experimental work here presented and its further analysis permits to draw the following conclusions:

- Austin's methodology has allowed us to characterize the kinetic behavior of tungsten ore by determining the kinetic parameters (α , α_T , ϕ_j , γ , β), concluding that the values S_i and B_{ij} do not vary significantly with time.
- The probability of fracture, S_i , is highest at 70% critical speed. Fracture function B_{ij} , does not vary significantly with mill speed. Nevertheless, it is affected by the feed particle size, becoming higher for coarser sizes.
- Equation (10) is proposed as the best α_T fit, specifically for the studied ore.
- Values of parameter γ are influenced by both mill speed and feed particle size. Coarser particles yield smaller γ values, i.e., they produce more fines, whereas finer particles produce lesser quantities. The parameters ϕ_j and β depend on the features of the ore.
- The chemical characterization and the study of the evolution of the relevant grinding parameters, such as P_{80} and R_r , to the grinding time have demonstrated that, first, the highest probability of fracture occurs at 70% of the critical speed and; second, the effect of differential grinding is evidenced between the W -bearing species and the gangue. The latter results in an increase of the W grade in the monosize 250/125 μm .

Author Contributions: Conceptualization and execution of experiments, J.V.N. and J.M.M.-A.; methodology and investigation, J.V.N. and A.L.C.-V.; formal analysis and data curation, J.V.N. and J.M.M.-A.; writing—original draft preparation, J.V.N.; writing—review and editing, J.V.N. and J.M.M.-A.; supervision, J.M.M.-A. and A.L.C.-V.; project administration and funding acquisition, J.M.M.-A. All authors have read and agreed to the submitted version of the manuscript.

Funding: This work is part of the OPTIMORE project funded by the European Union Horizon 2020 Research and Innovation Programme under grant agreement No 642201.

Institutional Review Board Statement: Not applicable.

Informed Consent Statement: Not applicable.

Data Availability Statement: No new data were created or analyzed in this study. Data sharing is not applicable to this article.

Conflicts of Interest: The authors declare no conflict of interest.

References

1. European Commission. Study on the EU's List of Critical Raw Materials. 2020. Available online: https://ec.europa.eu/commission/presscorner/detail/en/ip_20_1542 (accessed on 25 November 2020).
2. Roskill. Tungsten. *Market Report*. 2020. Available online: <https://roskill.com/market-report/tungsten/> (accessed on 25 November 2020).

3. Schmidt, S. *From Deposit to Concentrate: The Basics of Tungsten Mining Part 2: Operational Practices and Challenges*; International Tungsten Industry Association: London, UK, 2012; pp. 1–20. Available online: http://www.itia.info/assets/files/newsletters/Newsletter_2012_06.pdf (accessed on 25 November 2020).
4. Ormonde Mining PLC. *Annual Report & Accounts 2018*; Issue 256353; Ormonde Mining PLC Co.: Meath, Ireland, 2018.
5. Murciego, A.; Álvarez-Ayuso, E.; Pellitero, E.; Rodríguez, M.A.; García-Sánchez, A.; Tamayo, A.; Rubio, J.; Rubio, F.; Rubin, J. Study of arsenopyrite weathering products in mine wastes from abandoned tungsten and tin exploitations. *J. Hazard. Mater.* **2011**, *186*, 590–601. [[CrossRef](#)] [[PubMed](#)]
6. Alfonso, P.; Castro, D.; Garcia-Valles, M.; Tarragó, M.; Tomasa, O.; Martínez, S. Recycling of tailings from the Barruecopardo tungsten deposit for the production of glass. *J. Therm. Anal. Calorim.* **2016**, *125*, 681–687. [[CrossRef](#)]
7. Fuerstenau, D.W.; Lutch, A.D.J.J. The effect of ball size on the energy efficiency of hybrid high-pressure roll mill/ball mill grinding. *Powder Technol.* **1999**, *105*, 199–204. [[CrossRef](#)]
8. Menéndez-Aguado, J.M.; Velázquez, A.L.C.; Tijonov, O.N.; Díaz, M.A.R. Implementation of energy sustainability concepts during the comminution process of the Punta Gorda nickel ore plant (Cuba). *Powder Technol.* **2006**, *170*, 153–157. [[CrossRef](#)]
9. Gupta, V.K.; Sharma, S. Analysis of ball mill grinding operation using mill power specific kinetic parameters. *Adv. Powder Technol.* **2014**, *25*, 625–634. [[CrossRef](#)]
10. Gupta, V.K. Determination of the specific breakage rate parameters using the top-size-fraction method: Preparation of the feed charge and design of experiments. *Adv. Powder Technol.* **2016**, *27*, 1710–1718. [[CrossRef](#)]
11. Öksüzoglu, B.; Uçurum, M. An experimental study on the ultra-fine grinding of gypsum ore in a dry ball mill. *Powder Technol.* **2016**, *291*, 186–192. [[CrossRef](#)]
12. Pedrayes, F.; Norniella, J.G.; Melero, M.G.; Menéndez-Aguado, J.M.; del Coz-Díaz, J.J. Frequency domain characterization of torque in tumbling ball mills using DEM modelling: Application to filling level monitoring. *Powder Technol.* **2018**, *323*, 433–444. [[CrossRef](#)]
13. Deniz, V. Influence of interstitial filling on breakage kinetics of gypsum in ball mill. *Adv. Powder Technol.* **2011**, *22*, 512–517. [[CrossRef](#)]
14. Chimwani, N.; Glasser, D.; Hildebrandt, D.; Metzger, M.J.; Mulenga, F.K. Determination of the milling parameters of a platinum group minerals ore to optimize product size distribution for flotation purposes. *Miner. Eng.* **2013**, *43–44*, 67–78. [[CrossRef](#)]
15. Lund, C.; Lamberg, P. Geometallurgy-A tool for better resource efficiency. *Met. Miner.* **2014**, *37*, 39–43.
16. Mwangi, A.-R. Development of a Geometallurgical Testing Framework for Ore Grinding and Liberation Properties. Ph.D. Thesis, Lulea University of Technology, Lulea, Sweden, 2016.
17. Mwangi, A.; Parian, M.; Lamberg, P.; Rosenkranz, J. Comminution modeling using mineralogical properties of iron ores. *Miner. Eng.* **2017**, *111*, 182–197. [[CrossRef](#)]
18. Little, L.; Mainza, A.N.; Becker, M.; Wiese, J. Fine grinding: How mill type affects particle shape characteristics and mineral liberation. *Miner. Eng.* **2017**, *111*, 148–157. [[CrossRef](#)]
19. Gupta, V.K. Effect of size distribution of the particulate material on the specific breakage rate of particles in dry ball milling. *Powder Technol.* **2017**, *305*, 714–722. [[CrossRef](#)]
20. Ciribeni, V.; Bertero, R.; Tello, A.; Puerta, M.; Avellá, E.; Paez, M.; Aguado, J.M.M. Application of the Cumulative Kinetic Model in the Comminution of Critical Metal Ores. *Metals* **2020**, *10*, 925. [[CrossRef](#)]
21. Hesse, M.; Popov, O.; Lieberwirth, H. Increasing efficiency by selective comminution. *Miner. Eng.* **2017**, *103–104*, 112–126. [[CrossRef](#)]
22. Deniz, V. The effect of mill speed on kinetic breakage parameters of clinker and limestone. *Cem. Concr. Res.* **2004**, *34*, 1365–1371. [[CrossRef](#)]
23. Petrakis, E.; Komnitsas, K. Improved Modeling of the Grinding Process through the Combined Use of Matrix and Population Balance Models. *Minerals* **2017**, *7*, 67. [[CrossRef](#)]
24. Austin, L. A Review—Introduction to the mathematical description of grinding as a rate process. *Powder Technol.* **1972**, *5*, 1–17. [[CrossRef](#)]
25. Austin, L.G.; Klimpel, R.R.; Luckie, P.T. *Process Engineering of Size Reduction: Ball Milling*; SME—AIME: New York, NY, USA, 1984.
26. Wang, X.; Gui, W.; Yang, C.; Wang, Y. Wet grindability of an industrial ore and its breakage parameters estimation using population balances. *Int. J. Miner. Process.* **2011**, *98*, 113–117. [[CrossRef](#)]
27. Petrakis, E.; Stamboliadis, E.; Komnitsas, K. Identification of Optimal Mill Operating Parameters during Grinding of Quartz with the Use of Population Balance Modeling. *KONA Powder Part. J.* **2017**, *34*, 213–223. [[CrossRef](#)]
28. Austin, L.G.; Brame, K. A comparison of the Bond method for sizing wet tumbling ball mills with a size—mass balance simulation model. *Powder Technol.* **1983**, *34*, 261–274. [[CrossRef](#)]
29. Steiner. Characterization of laboratory-scale tumbling mills. *Int. J. Miner. Process.* **1996**, *44–45*, 373–382.
30. Herbst, J.A.; Fuerstenau, D.W. Mathematical simulation of dry ball milling using specific power information. *Trans. AIME* **1973**, *254*, 343–348.
31. Cayirli, S. Influences of operating parameters on dry ball mill performance. *Physicochem. Probl. Miner. Process.* **2018**, *54*, 751–762.
32. Ipek, H.; Goktepe, F. Determination of grindability characteristics of zeolite. *Physicochem. Probl. Miner. Process.* **2011**, *47*, 183–192.